International Journal of Smart and Nano Materials

Publication details, including instructions for authors and subscription information:
http://www.tandfonline.com/loi/tsnm20

An artificial lateral line system using IPMC sensor arrays

Ahmad T. Abdulsadda [a] & Xiaobo Tan [a]

[a] Smart Microsystems Laboratory, Department of Electrical and Computer Engineering, Michigan State University, East Lansing, MI, 48824, USAJanuary 9, 2012

Version of record first published: 20 Jan 2012.

To cite this article: Ahmad T. Abdulsadda & Xiaobo Tan (2012): An artificial lateral line system using IPMC sensor arrays, International Journal of Smart and Nano Materials, 3:3, 226-242

To link to this article: http://dx.doi.org/10.1080/19475411.2011.650233

International Journal of Smart and Nano Materials
Vol. 3, No. 3, September 2012, 226–242

An artificial lateral line system using IPMC sensor arrays

Ahmad T. Abdulsadda and Xiaobo Tan*

Smart Microsystems Laboratory, Department of Electrical and Computer Engineering, Michigan State University, East Lansing, MI 48824 USA January 9, 2012

(*Received 30 September 2011; final version received 4 December 2011*)

Most fish and aquatic amphibians use the lateral line system, consisting of arrays of hair-like neuromasts, as an important sensory organ for prey/predator detection, communication, and navigation. In this paper a novel bio-inspired artificial lateral line system is proposed for underwater robots and vehicles by exploiting the inherent sensing capability of ionic polymer–metal composites (IPMCs). Analogous to its biological counterpart, the IPMC-based lateral line processes the sensor signals through a neural network. The effectiveness of the proposed lateral line is validated experimentally in the localization of a dipole source (vibrating sphere) underwater. In particular, as a proof of concept, a prototype with body length (BL) of 10 cm, comprising six millimeter-scale IPMC sensors, is constructed and tested. Experimental results have shown that the IPMC-based lateral line can localize the source from 1–2 BLs away, with a maximum localization error of 0.3 cm, when the data for training the neural network are collected from a grid of 2 cm by 2 cm lattices. The effect of the number of sensors on the localization accuracy has also been examined.

Keywords: ionic polymer–metal composite (IPMC); lateral line system; neural networks; flow sensing; dipole source localization

1. Introduction

Most fish and aquatic amphibians use the lateral line system as an important sensory organ to probe their environments [1, 2]. A lateral line consists of arrays of hair cell sensors, known as neuromasts. Each neuromast contains bundles of sensory hairs, encapsulated in a gelatinous structure called a cupula. An impinging flow deflects the cupula, and thus the hairs inside, eliciting firing of the hair cell neurons. Neuromasts can be divided into two types, superficial neuromasts, which are distributed on the skin surf[l]ace, and canal neuromasts, which are recessed in the scales or in bony canals underneath the skin. With the same basic structure, the two types of neuromasts show distinct sensing characteristics [3]. The lateral line system allows an aquatic animal to identify near-field objects of interest and perform hydrodynamic imaging of the environment, typically within one to two body lengths (BLs) of the animal. Consequently, the lateral line is involved in various behaviors of aquatic animals, such as prey/predator detection [4], schooling [5], rheotaxis [6], courtship and communication [2]. In addition to the qualitative roles the lateral line plays in behavior, there have been studies on how probed information is encoded and decoded in the nervous systems [7].

*Corresponding author. Email: xbtan@egr.msu.edu (X.T.)

ISSN 1947-542X online

http://dx.doi.org/10.1080/19475411.2011.650233
http://www.tandfonline.com

The biological lateral line system has inspired the effort to engineer artificial lateral lines for applications in underwater vehicles and robots. As a stealthy complement to existing sensing modules, such as cameras and sonars, artificial lateral lines can potentially provide information on flow conditions, obstacles, and moving objects for underwater robots and vehicles. This in turn can enable obstacle-avoidance, energy-saving in locomotion, collaborative behavior such as schooling, and stabilization in response to turbulent currents or choppy waves. On the hardware side, arrays of flow sensors, explicitly motivated by the biological lateral line, have been fabricated based on various transduction principles, such as hot-wire anemometry 8, piezoresistivity/strain gauges [9, 10], and capacitive sensing [11].

On the signal processing side, researchers have mainly examined the problem of localizing a vibrating sphere, known as a dipole. Dipole sources have been extensively used in physiological and behavioral studies of biological lateral lines, since they provide simple emulation of tail-beating or appendage movement of aquatic animals, and analytical expressions of the resulting flow field are available [12]. Consequently, dipole source localization has become a natural starting point for studying artificial lateral lines. Dagamseh *et al.* proposed the use of characteristic points (zero-crossings, maxima, etc.) in the measured velocity profile for dipole source localization [11], similar to what was proposed by Franosch *et al.* for modeling the localization by the clawed frog *Xenopus* [13]. However, this approach would require prohibitively many sensors to determine the characteristic points, and it is limited to a maximum detection distance of $1/\sqrt{2}$ BL. Data-matching approaches were presented by Pandya *et al.*, where the measured signal pattern was compared with a large, pre-obtained set of templates or a model fitted with a sufficient amount of data [14]. These approaches suffered from the need for excessive computing and storage resources, or the difficulty in system-level implementation [14]. Recently, a beam-forming algorithm for array signal processing was used to localize a dipole source and a flicking fish tail [10]. With a sensor–source separation of 0.5 BL, the resulting mean estimation error is between 0.1 and 0.2 BL.

The contribution of this paper is a novel approach to the realization of artificial lateral lines, which exploits the inherent sensing properties of ionic polymer–metal composites (IPMCs) [15, 16]. An IPMC has three layers, with an ion-exchange polymer membrane sandwiched between metal electrodes. Inside the polymer, (negatively charged) anions covalently fixed to polymer chains are balanced by mobile (positively charged) cations. Deformation under a mechanical perturbation redistributes the cations, producing a detectable electric signal (e.g., short-circuit current) that is well correlated with the mechanical stimulus, which explains the sensing principle of an IPMC. Conversely, under an applied voltage, transport of hydrated cations and water molecules within the membrane, together with the associated electrostatic interactions, leads to bending motion of the IPMC sample. Many researchers have studied the fabrication [17–19], characterization, and modeling [20–29] of IPMC sensors and actuators. Recent years have seen significant interest in using IPMC materials for underwater actuation [30–36], sensing [37], and energy harvesting [38].

We have chosen the IPMC material for creating artificial lateral lines in this work for several reasons. First, IPMCs work well in water and have direct mechanosensory properties, which makes it relatively easy to construct the sensor and its readout circuitry. Another advantage of IPMC sensors (over, e.g., hot-wire flow sensors) is that they automatically capture the flow polarity. Furthermore, the softness of IPMC material allows it to respond to small flows and thus attain high measurement sensitivity. Finally, the fabrication processes for IPMCs are relatively simple and have been studied extensively over the past

decade. In particular, for millimeter-scale and above, one can fabricate an IPMC sheet using well-known processes [17] and then cut it into any desired sizes.

In this paper we propose an artificial neural network-based scheme for processing the signals from IPMC sensor arrays, to localize a dipole source. In general, the relationship between the source location and the resulting flow field (and thus the sensor outputs) is highly nonlinear and complex. While there is an analytical but nonlinear model for a dipole-generated flow field under ideal assumptions [12], this model may not capture the flow field well under more realistic conditions, an example of which is the frequent scenario that involves fluid–structure interactions. Artificial neural networks are capable of approximating nonlinear mappings, and in particular, when such mappings are unknown, there are established methods for training the approximating neural networks [39]. For this reason, we have adopted a neural network-based scheme for the dipole source localization.

The concept of an IPMC lateral line and its neural network-based processing scheme are examined experimentally. A prototype comprising six millimeter-scale IPMC sensors, with a body length (BL) of 10 cm, is constructed. The localization experiments are conducted for a dipole source that is vibrating at 40 Hz. Note that this frequency is consistent with the typical range of dipole frequencies adopted in the study of biological and artificial lateral lines (e.g., 50 Hz in [40] and 45 Hz in [10,41]). Experimental results show that the IPMC-based lateral line can localize the dipole source 1–2 BLs away, with a maximum localization error of 0.3 cm, when the data for training the neural network are collected from a grid of 2 cm by 2 cm lattices. The performance of the lateral line using fewer sensors is also studied, and it is found that, with fewer sensors, more training data are needed to achieve a given localization precision. For example, when four sensors are used, it requires training data on a grid of 1 cm by 1 cm lattices to yield the same level of localization accuracy as achieved by six sensors with training data from 2×2 cm^2 lattices. These results have not only demonstrated the feasibility of using arrays of IPMC sensors as artificial lateral lines, but also provided interesting insight into the trade-offs in design and implementation.

The remainder of the paper is organized as follows. The neural network-based processing scheme is described in Section 2. The experimental setup and basic sensor characterization are presented in Section 3. Experimental results on the localization of a dipole source are presented in Section 4. Finally, concluding remarks are provided in Section 5.

2. Source localization using neural network processing

In this work we consider the localization of a dipole source in a two-dimensional (2D) plane with coordinates (x, y). The proposed approach can be extended readily to localization in 3D space, although that will require more training points for the neural network. Figure 1 illustrates the problem setup. Here (x, y) denotes the location of the source, and the IPMC sensor arrays are placed at a known location.

The signals from IPMC sensors of the artificial lateral line are complex functions of the source location. Even for the dipole stimulation, the flow field measured with digital particle image velocimetry (DPIV) deviates appreciably from the theoretical predictions, because of non-ideal fluid conditions and interactions of the fluid with structures (e.g., with the IPMC beams and the walls of the tank). In addition, the sensing characteristics of individual sensors could be different from each other in practice because of imperfect fabrication processes. The sensor outputs are further contaminated with noise due to ambient water movement and thermal fluctuations [37]. As a result, it is difficult to decode the sensor signals analytically.

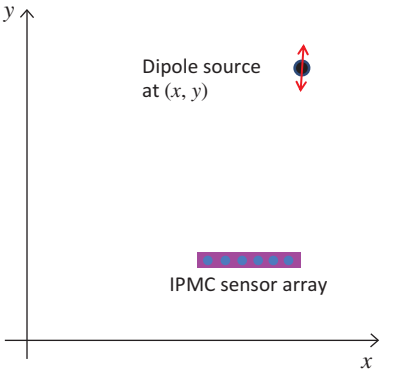

Figure 1. Schematic of the dipole source localization problem.

Biological fish are faced with similar challenges in extracting relevant sensing information from a vast amount of data that are corrupted by noise. However, they manage to accomplish source localization and other missions robustly through neural network-based information processing. Taking this biological inspiration, we construct an (artificial) neural network to process the signals acquired by the IPMC-based lateral line. As illustrated in Figure 2, we adopt the multilayer perceptron (MLP) architecture for the neural network. An MLP network consists of an input layer, a hidden layer, and an output layer, and is the most widely used network structure for nonlinear classification and prediction applications [39].

One could use different features extracted from the sensor output data as the input to the neural network. In this work, we use the signal amplitude at the stimulus frequency because of its robustness to measurement noise. The amplitude is obtained through the fast Fourier transform (FFT) of the raw sensor signal. The number of inputs is the same as the number of IPMC sensors considered. For comparison purposes, in this work we investigate the performance of the artificial lateral line when different numbers of sensors are adopted. The number of hidden-layer nodes is chosen through a genetic algorithm (GA)-based optimization process, which will be further described below. Each hidden-layer node represents the operation of nonlinear activation, which takes the form of a sigmoid function. The output layer has two nodes, representing the x and y coordinates of the vibrating source.

The number of hidden-layer nodes and the connective weights between the layers are determined through a two-phase training procedure, using the software

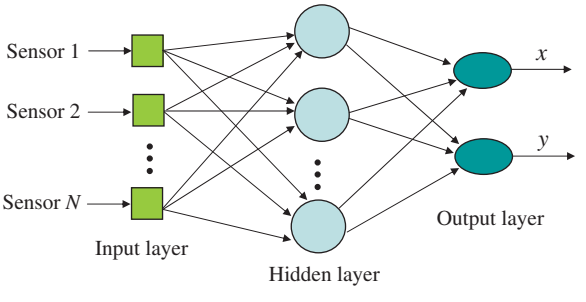

Figure 2. Schematic of the MLP neural network for signal processing of the IPMC lateral line.

NeuroSolutions [42]. The training data are obtained by placing the stimulus at known locations (x_i, y_i), $1 \leq i \leq M$, measuring the corresponding sensor outputs and computing the signal amplitudes. In the first training phase, a genetic algorithm is used to find an appropriate value for the number of hidden-layer nodes and a reasonable set of values for the connective weights. In particular, each genome encodes both the number of hidden-layer nodes and the weights of all connecting edges. The maximum number of hidden-layer nodes is limited to 24 based on the number of network inputs and outputs. We consider a population size of 40 genomes and run 25 generations of evolution (crossover/mutation). The fitness function (or more appropriately, the cost function) used in the selection process is the mean square error J:

$$J = \frac{1}{2M} \sum_{i=1}^{M} \left(x_i - \hat{x}_i\right)^2 + \left(y_i - \hat{y}_i\right)^2, \tag{1}$$

where $(\hat{x}_i, \hat{y}_i)$ denotes the predicted value for (x_i, y_i) under the current network structure and weights.

The values of the connective weights obtained in the first training phase then serve as the initial condition for weight refinement in the second phase, where the network structure is fixed as determined in the first phase. Delta-bar-delta learning [39], with an adaptive learning rate, is used for weight optimization. Let K be the total number of weights. For each weight w_k, $1 \leq k \leq K$, the update rule is

$$w_k^{\text{new}} = w_k^{\text{old}} - \eta_k^{\text{new}} \frac{\partial J}{\partial w_k^{\text{old}}}, \tag{2}$$

where the adaptive learning rate η_k is updated as

$$\eta_k^{\text{new}} = \begin{cases} \eta_k^{\text{old}} + a, & \text{if } \dfrac{\partial J}{\partial w_k^{\text{old}}} > 0 \\ b\eta_k^{\text{old}}, & \text{if } \dfrac{\partial J}{\partial w_k^{\text{old}}} \leq 0, \end{cases} \tag{3}$$

and a, b are constants satisfying $0 < a, b < 1$.

3. Experimental setup and sensor characterization

Figure 3 shows the constructed lateral line prototype, consisting of six IPMC sensors. Each sensor, with dimensions 8 mm × 2 mm × 200 μm, has been cut from an IPMC sheet fabricated by the Smart Microsystems Laboratory at Michigan State University, following a recipe similar to the one described in [43]. The IPMC material contains lithium ions (Li^+) as cations. The sensor-to-sensor separation is 2 cm, resulting in a total span of 10 cm, which will be regarded as the body length (BL) in later discussions.

Under a mechanical stimulus, an open-circuit voltage or a short-circuit current can be measured across the two electrodes of an IPMC. We have chosen to take the short-circuit current as the sensor output because current measurement is less susceptible to noise. Figure 4 shows a schematic of the measurement circuit, which consists of two cascaded operational amplifiers (op-amps) [37]. A low-noise, low-bias precision op-amp (OPA 124 from Texas Instruments) is adopted for the first-tier amplification, to reduce both the

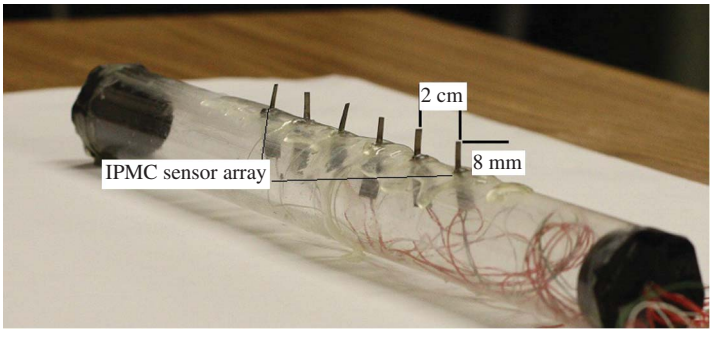

Figure 3. A prototype of an IPMC-based lateral line system.

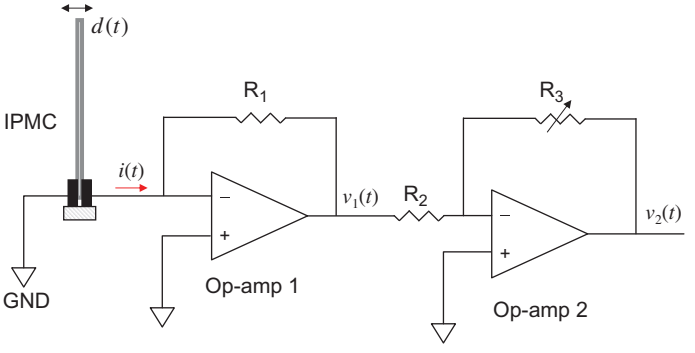

Figure 4. A schematic of the circuit for measuring the short-circuit current generated by the IPMC sensor.

noise and the spurious DC bias in the sensor output induced by the leakage current. Since the "–" terminal of Op-amp 1 is virtually the ground (following standard op-amp circuit analysis), the two electrodes of the IPMC can be considered short-circuited. The sensing current generated under this configuration, $i(t)$, is proportional to the voltage output $v_1(t) = R_1 i(t)$. The second op-amp is introduced for gain adjustment, where the resistor R_3 is tunable. The output $v_2(t)$ is related to the current signal $i(t)$ via $v_2(t) = \frac{R_3 R_1}{R_2} i(t)$. In the circuit we used, $R_1 = 470\text{k}\Omega$, $R_2 = 10\text{k}\Omega$, and R_3 was adjustable from 0 to 50 . Acquisition and processing of the IPMC sensor output are conducted through a dSPACE system (DS1104, dSPACE Inc., Germany). A digital low-pass filter with cutoff frequency 55 Hz is further implemented to remove high-frequency noise from the sensor signals.

All experiments are conducted in a water tank, shown in Figure 5(a). The tank measures $6 \times 2 \times 2$ ft^3, and is equipped with a digital particle image velocimetry (DPIV) system (LaVision, Ypsilanti, MI). In a DPIV system, small particles are dispersed in a fluid and a laser sheet is created in the fluid to illuminate the particles. Processing of images taken in quick successions can reveal the movement of particles and thus provide information about the flow field. In our experiments, the DPIV system is used for preliminary characterization of the flow field under the stimulating source. A dipole source is created with a mini-shaker (4810, Brüel & Kjaer, Denmark) (Figure 5b), the vibration amplitude and frequency of which can be readily controlled through a voltage input to the shaker. A lightweight bar firmly attached to the mini-shaker then translates the vibration to a sphere rigidly coupled to the bar. The sphere, which is a steel ball, has a diameter of 19 mm. The frequency range

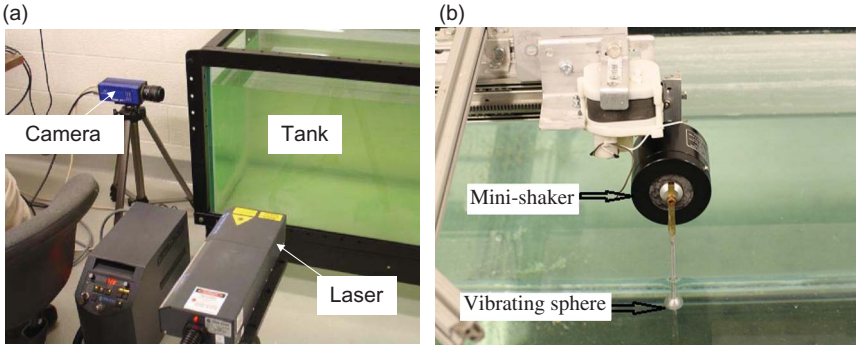

Figure 5. Experimental setup: (a) Experimental tank equipped with a DPIV system; (b) the mini-shaker-based dipole source.

of the dipole spans DC–20 kHz. The source location and vibration direction with respect to the IPMC lateral line can be adjusted by moving the stand holding the IPMC lateral line or by moving the source itself.

DPIV experiments have been conducted to observe the flow field around the IPMC sensors, for different source–sensor separation, to get a sense of the flow magnitude under the stimuli. For example, Figure 6 shows the flow fields around an IPMC sensor for a 19 mm × 14 mm window, under a 20 Hz stimulus produced with a dipole source described in [37], where both the source vibration axis and the illuminated plane are perpendicular to the IPMC beam plane. In other words, the IPMC beam would bend left and right in Figure 6, although the IPMC thickness did not look to scale because of laser light scattering around the beam. Figures 6(a) and (b) correspond to dipole–IPMC separations of 10 and 45 cm, respectively, which clearly indicates that the flow velocity decreases as the separation between source and sensor increases.

Figure 7 shows typical sensor responses under the mini-shaker-based stimulation (40 Hz), indicating that the current output from the IPMC sensor is of the order of μA, which can be captured very well by the sensing circuit. Figure 7(a) shows the signal from sensor #2 of the IPMC lateral line, when the source is 1 cm away from this sensor, while Figure 7(b) shows the response from sensor #4 (4 cm from sensor #2) under the same stimulus. In this experiment the lateral line axis is perpendicular to the vibration axis of the dipole source, and perpendicular to the beam plane of each sensor.

Figure 8 shows the amplitude of the signal from one IPMC, located at (7,0), as a function of the location (x, y) of the mini-shaker-based dipole stimulus. It can be seen that, while in general the signal gets stronger when the source gets closer, the overall amplitude landscape has a sophisticated profile. The results in Figure 8 clearly illustrate the challenge in underwater localization. In particular, it would be difficult to localize unambiguously a source with a single sensor; instead, a lateral line-like array structure will be needed.

4. Experimental results on dipole source localization

As shown in Figure 10, a working area of about 20×10 cm^2 is used in the experiments. The frequency of the dipole source is 40 Hz, and the vibration is along the y direction with an amplitude of 1.91 mm. The lateral line is placed in parallel with the x-axis, at

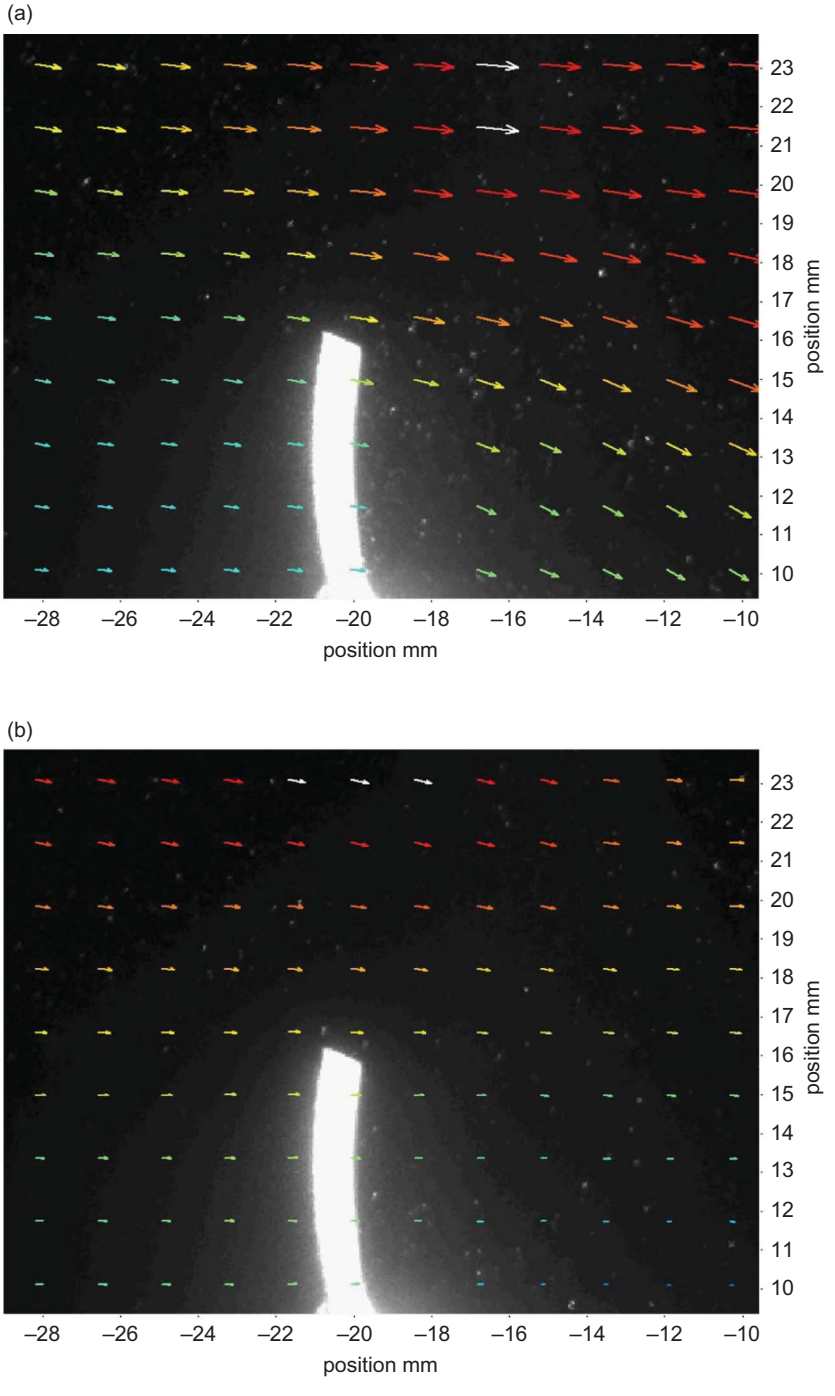

Figure 6. Flow field around one IPMC sensor under a dipole stimulation: (a) Dipole–sensor separation 10 cm, with maximum flow amplitude of 9.3 mm/s in the field; (b) dipole–sensor separation 45 cm, with maximum flow amplitude of 4.1 mm/s in the field.

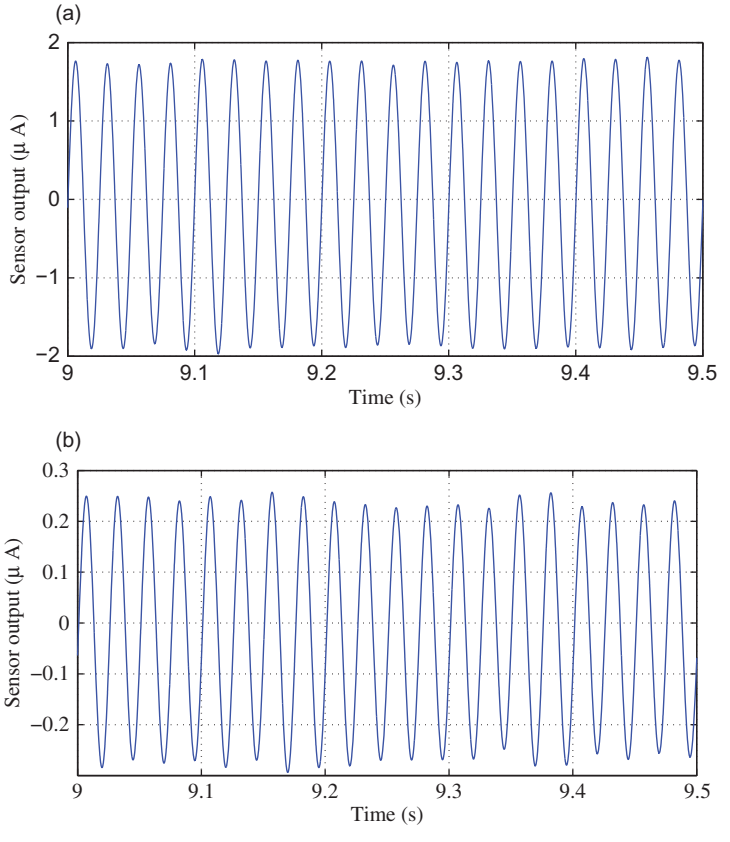

Figure 7. Typical IPMC sensor signals: (a) Signal from sensor #2, which is close to the dipole source; (b) signal from sensor #4.

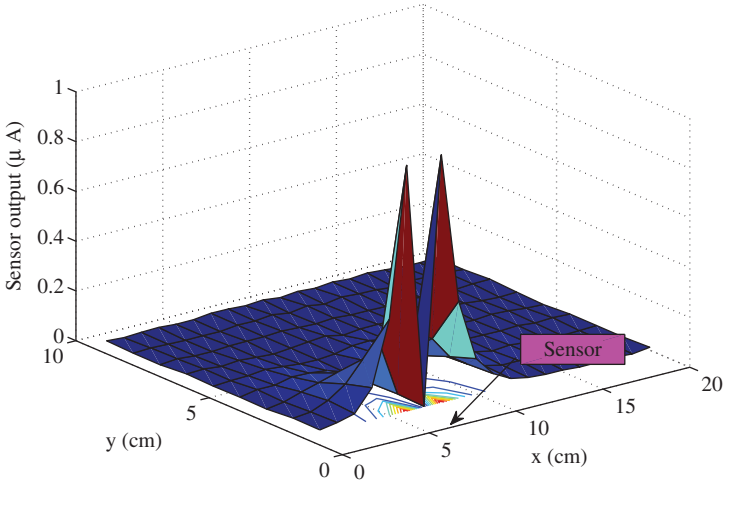

Figure 8. Sensor characterization: measured sensor signal magnitude as a function of source location, where the dipole vibration axis is parallel to the IPMC beam plane.

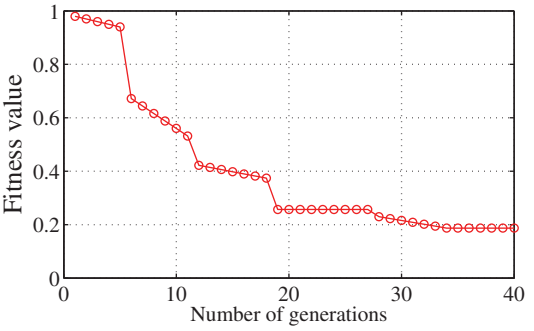

Figure 9. Evolution of the fitness function (the mean square error J) over generations, in the genetic algorithm-based training phase. This example involves all six sensors and 180 training points.

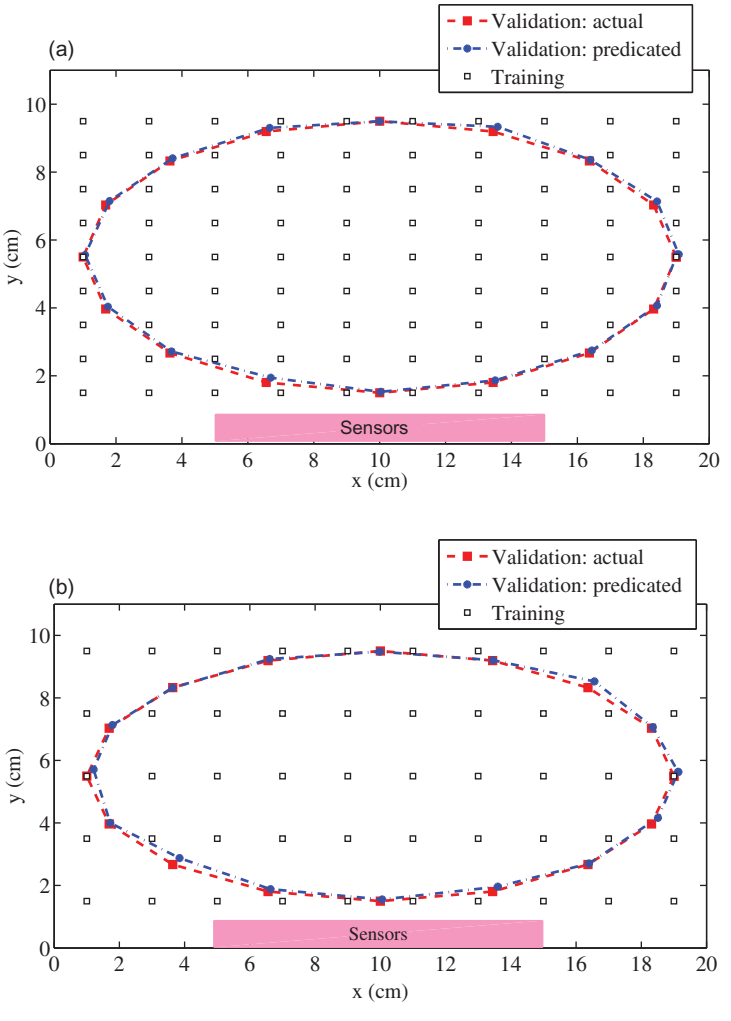

Figure 10. Localization of the dipole source using all six sensors of the lateral line: (a) With 90 training points; (b) with 50 training points.

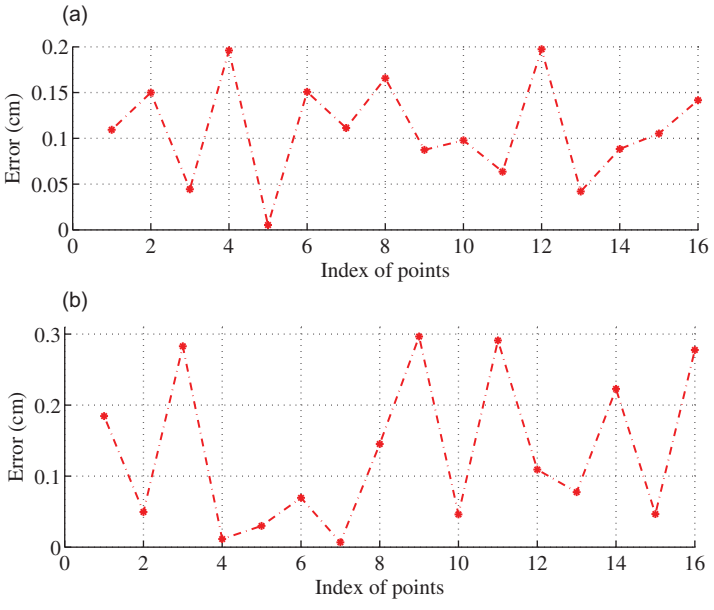

Figure 11. Localization error at 16 validation points when all six sensors are used: (a) With 90 training points; (b) with 50 training points.

$y = 0$ and spanning from $x = 5$ cm to $x = 15$ cm. The beam plane of each IPMC sensor is perpendicular to the lateral line direction. Both the dipole source and the lateral line are placed 6 cm underwater. First, for the purpose of training the neural network, we define a grid of $1 \times 1\text{cm}^2$ lattices in the working area, resulting in a total of 180 grid points. The dipole source is placed at each grid point, where the amplitude of the signal from each IPMC sensor in the lateral line is obtained. Subsets of these data are used to train the neural network in different cases. Figure 9 shows the evolution of the cost function J in (1) during the first, genetic algorithm-based training phase, for the case involving six sensors and 180 training points. It can be seen that the cost function converges to a steady-state value as the number of generations approaches 40. As explained in Section 2, the connective weights obtained in the first training phase are then refined in the second phase using delta-bar-delta learning. To test the performance of the lateral line, we place the dipole source at each of 16 points along an elliptical track centered at (10, 5.5), obtain the amplitudes of sensor signals from the lateral line and feed them to the trained neural network, and compare the output of the network to the actual location.

Figures 10(a) and (b) show the localization results when all six sensors are used, where 90 ($2 \times 1\text{cm}^2$ lattices) and 50 ($2 \times 2\text{cm}^2$ lattices) training points are utilized, respectively. The locations of the training points are denoted with squares in the figures. Figures 11(a) and (b) further show the actual localization errors at all 16 validation points for the two cases. It is clear from Figure 11(b) that, for a training grid of 2×2 cm^2 lattices (50 points), the maximum localization error is 0.3 cm. The maximum error drops to 0.2 cm when the number of training points is increased to 90 (Figure 11a). Note that the resulting neural networks are different when different numbers of training points (or different numbers of sensors) are used. For example, the neural network has 13 hidden nodes for the case in Figure 10(a), while it has 10 hidden nodes for the case in Figure 10(b).

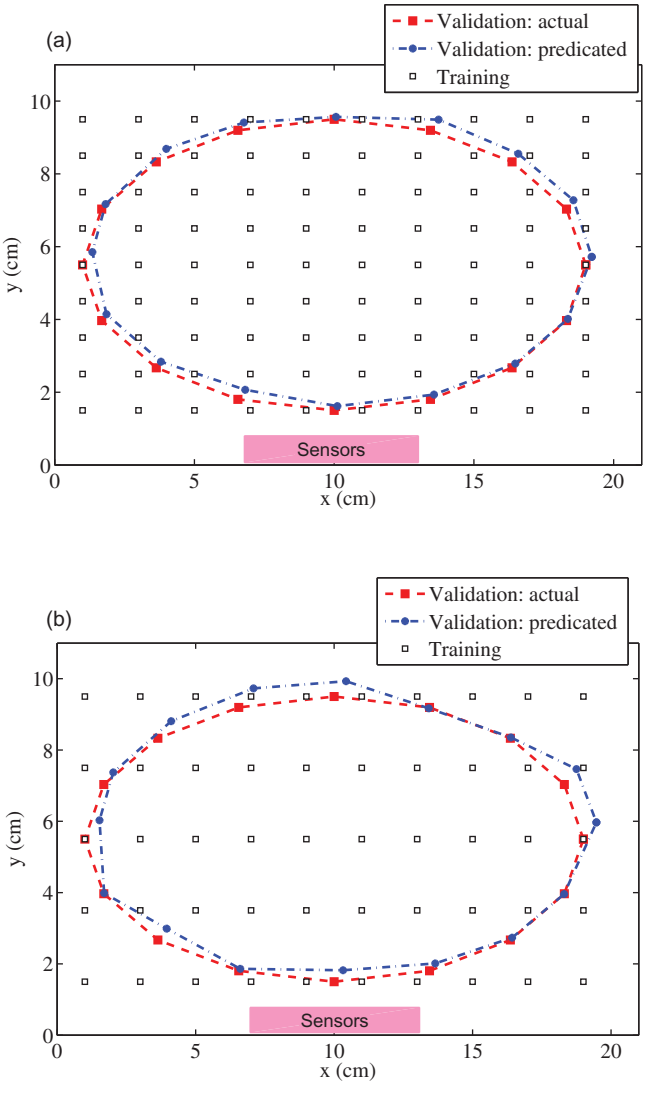

Figure 12. Localization of the dipole source using four sensors of the lateral line: (a) With 90 training points; (b) with 50 training points.

In order to examine the effect of the number of sensors on the localization performance, we have repeated the localization with four and two sensors of the lateral line, as shown in Figures 12 and 13, respectively. In each case, the sensors are taken from the middle section of the lateral line. It is clear that with fewer sensors, the localization error increases. Figure 14 further shows the maximum and average localization errors when different numbers of sensors and training points are used. From the figure, we can see that the localization performance with four sensors becomes comparable to that with six sensors when the number of training points is quadrupled (from 2×2 cm^2 lattices to 1×1 cm^2 lattices); and for two sensors, even with all 180 training points, the maximum localization error is bigger than that with all six sensors when only 25 training points are used.

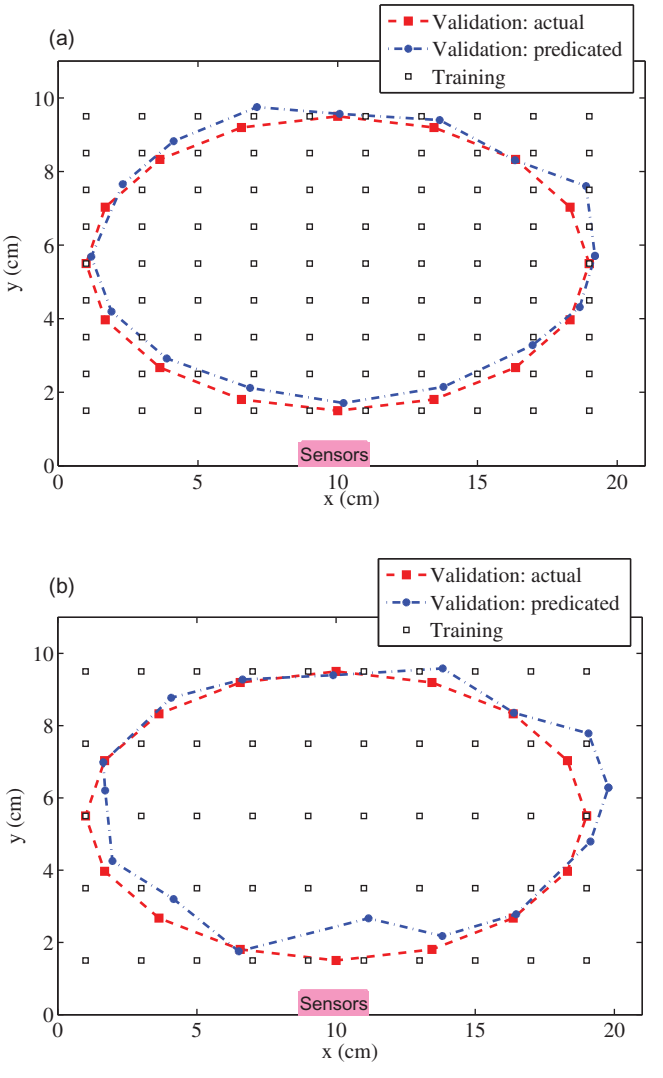

Figure 13. Localization of the dipole source using two sensors of the lateral line: (a) With 90 training points; (b) with 50 training points.

5. Conclusions

The contribution of this paper was a new approach to the realization of artificial lateral lines for underwater robots and vehicles, including both the proposal of using IPMC materials as sensing elements and the neural network-based signal processing algorithm. The effectiveness of the proposed approach was validated in experiments involving localization of a dipole source. Experimental results showed that, with relatively few sensor elements, the IPMC-based lateral line was able to localize sources at least 1–2 BLs away, and the localization accuracy at source–sensor separation of 1 BL was comparable to the resolution of manually placing the source (1–2 mm).

Although this work has demonstrated the promise of IPMC sensors in underwater flow sensing, we note that the behavior of IPMCs depends on environmental conditions and

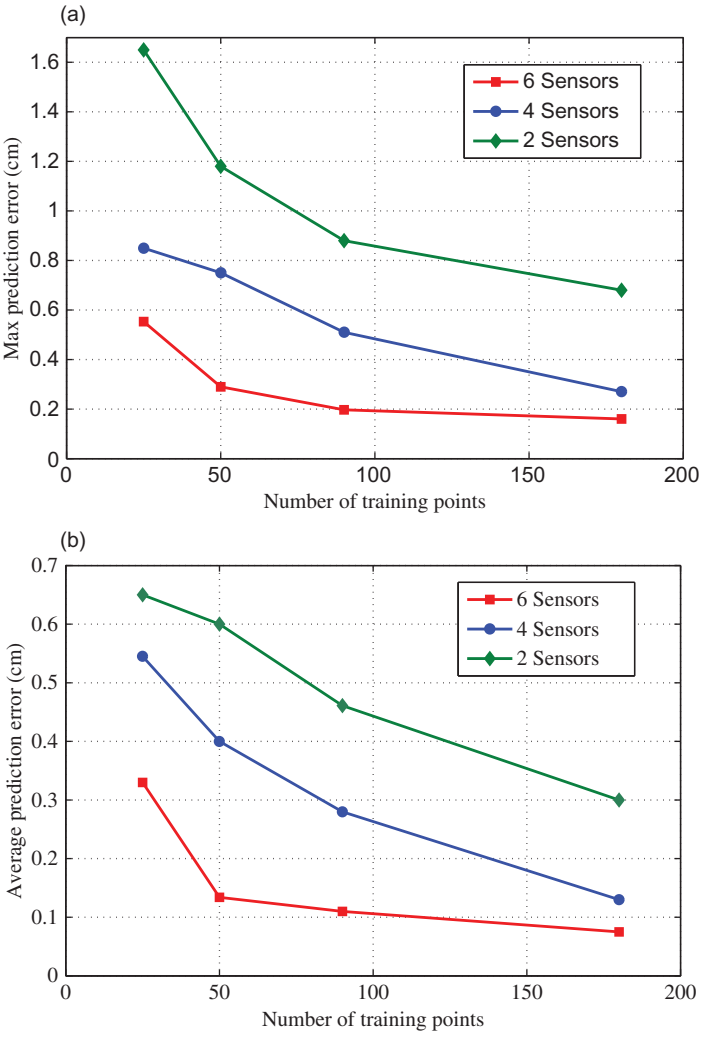

Figure 14. Error in localization of the dipole source using the lateral line: (a) Maximum error along the track; (b) average error along the track.

could vary over time. While the continuing advances in IPMC fabrication may alleviate such problems, appropriate compensation schemes (see, e.g., [37]) and periodic sensor calibrations are expected to be essential for practical IPMC lateral line systems.

Compared to the size (less than 1 mm long) of neuromasts in a biological lateral line, the IPMC sensors used in this paper are relatively big. In addition, a biological lateral line may have many more (from tens to over a thousand [1]) neuromasts. There are many challenges in realizing an IPMC-based artificial lateral line system with sensor size and number comparable to those of a live fish. For example, while the processes for microfabrication of IPMCs have been reported by a number of groups [19,44,45], existing results deal mostly with planar processes, and new polymer MEMS techniques have to be developed to create micro-IPMC devices standing on a substrate. In addition, on the system integration side, the processing of signals from tens to hundreds of IPMC sensors is far from trivial.

To address this challenge, it will be critical to seek inspiration from how such processing is achieved in biology [2].

The work reported in this paper will be extended in several directions. First, we note that in this work the FFT was used to extract the signal amplitude. Consequently, the signal processing approach is not amenable to online implementation. To address this problem, we will use a sliding discrete Fourier transform (SDFT) [46,47] to update the signal amplitude as new data samples come in. This will not only allow us to perform source localization in real time, but will also enable the tracking of a moving dipole source, where the received signal amplitude is time-varying. Second, we will mount the IPMC-based lateral line on a swimming robotic fish, and investigate the processing schemes for the lateral line to decouple external signals from self-motion-induced flow signals.

Acknowledgments

This work was supported in part by the National Science Foundation (ECCS 0547131, CCF 0820220, IIS 0916720) and the Office of Naval Research (Grant N000140810640). The authors would like to thank Feitin Zhang for assisting in conducting the DPIV experiments, Hong Lei for preparing the IPMC material used in this work, and Prof. Sheryl Coombs for making the mini-shaker available to us for conducting the experiments.

References

[1] S. Coombs, *Smart skins: Information processing by lateral line flow sensors*, Auton. Robots 11 (2001), pp. 255–261.
[2] S. Coombs and C.B. Braun, *Information processing by the lateral line system*, in *Sensory processing in aquatic environments*, S.P. Collin and N.J. Marshall, eds., Springer-Verlag, New York, 2003, chap. 7, pp. 122–138.
[3] A.B.A. Kroese and N.A.M. Schellart, *Velocity- and acceleration-sensitive units in the trunk lateral line of the trout*, J. Neurophys. 68 (1992), pp. 2212–2221.
[4] K. Pohlmann, J. Atema, and T. Breithaupt, *The importance of the lateral line in nocturnal predation of piscivorous catfish*, J. Exper. Biol. 207 (2004), pp. 2971–2978.
[5] T. Pitcher, B.L. Partridge, and C.S. Wardle, *A blind fish can school*, Science 194 (1976), pp. 963–965.
[6] J.M. Gardiner and J. Atema, *Sharks need the lateral line to locate odor sources: Rheotaxis and eddy chemotaxis*, J. Exper. Biol. 210 (2007), pp. 1925–1934.
[7] B. Curcic-Blake and S.M. van Netten, *Source location encoding in the fish lateral line canal*, J. Exper. Biol. 209 (2006), pp. 1548–1559.
[8] Y. Yang, J. Chen, J. Engel, S. Pandya, N. Chen, C. Tucker, S. Coombs, D.L. Jones, and C. Liu, *Distant touch hydrodynamic imaging with an artificial lateral line*, Proc. Natl Acad. Sci. USA 103 (2006), pp. 18891–18895.
[9] V.I. Fernandez, S.M. Hou, F.S. Hover, J.H. Lang, and M. Triantafyllou, *Development and application of distributed MEMS pressure sensor array for AUV object avoidance*, in *Proceedings of the Unmanned Untethered Submersible Technology Symposium*, Durham, NH, 2009.
[10] Y. Yang, N. Nguyen, N. Chen, M. Lockwood, C. Tucker, H. Hu, H. Bleckmann, C. Liu, and D.L. Jones, *Artificial lateral line with biomimetic neuromasts to emulate fish sensing*, Bioinspiration and Biomimetics 5 (2010), pp. 016001:1–9.
[11] A. Dagamseh, T. Lammerink, M. Kolster, C. Bruinink, R. Wiegerink, and G. Krijnen, *Dipole-source localization using biomimetic flow-sensor arrays positioned as lateral-line system*, Sensors and Actuators A 162 (2010), pp. 355–360.
[12] H. Lamb, *Hydrodynamics*, Cambridge University Press, Cambridge, 1932.
[13] J.M.P. Franosch, A.B. Sichert, M.D. Suttner, and J.L. van Hemmen, *Estimating position and velocity of a submerged moving object by the clawed frog Xenopus and by fish: A cybernetic approach*, Biol. Cybern. 93 (2005), pp. 231–238.
[14] S. Pandya, Y. Yang, D.L. Jones, J. Engel, and C. Liu, *Multisensor processing algorithms for underwater dipole localization and tracking using MEMS artificial lateral-line sensors*, EURASIP J. Appl. Signal Process. (2006) Article ID 76593. doi:10.1155/ASP/2006/76593.

[15] M. Shahinpoor and K. Kim, *Ionic polymer–metal composites: I. Fundamentals*, Smart Mater. Struct. 10 (2001), pp. 819–833.

[16] Z. Chen, X. Tan, A. Will, and C. Ziel, *A dynamic model for ionic polymer–metal composite sensors*, Smart Mater. Struct. 16 (2007), pp. 1477–1488.

[17] K. Kim and M. Shahinpoor, *Ionic polymer–metal composites: II. manufacturing techniques*, Smart Mater. Struct. 12 (2003), pp. 65–79.

[18] B. Akle, M. Bennett, and D. Leo, *High-strain ionomeric-ionic liquid electroactive actuators*, Sensors and Actuators A 126 (2006), pp. 173–181.

[19] Z. Chen and X. Tan, *Monolithic fabrication of ionic polymer–metal composite actuators capable of complex deformation*, Sensors and Actuators A: Physical 157 (2010), pp. 246–257.

[20] S. Nemat-Nasser and J. Li, *Electromechanical response of ionic polymer–metal composites*, J. Appl. Phys. 87 (2000), pp. 3321–3331.

[21] K. Takagi, Y. Nakabo, Z. Luo, T. Mukai, M. Yamamura, and Y. Hayakawa, *An analysis of the increase of bending response in IPMC dynamics given uniform input*, in *Smart Structures and Materials 2006: Electroactive Polymer Actuators and Devices (EAPAD)*, Vol. 6168 of *Proc. SPIE*, San Diego, CA, 2006, p. 616814.

[22] C. Bonomo, L. Fortuna, P. Giannone, S. Graziani, and S. Strazzeri, *A model for ionic polymer–metal composites as sensors*, Smart Mater. Struct. 15 (2006), pp. 749–758.

[23] Z. Chen and X. Tan, *A control-oriented and physics-based model for ionic polymer–metal composite actuators*, IEEE/ASME Trans. Mechatronics 13 (2008), pp. 519–529.

[24] Z. Chen, D. Hedgepeth, and X. Tan, *A nonlinear, control-oriented model for ionic polymer–metal composite actuators*, Smart Mater. Struct. 18 (2009), 055008:1–9.

[25] P. Gennesde, K. Okumura, M. Shahinpoor, and K. Kim, *Mechanoelectric effects in ionic gels*, Europhys. Lett. 50 (2000), pp. 513–518.

[26] M. Porfiri, *Charge dynamics in ionic polymer–metal composites*, J. Appl. Phys. 104 (2008), 104915:1–10.

[27] D. Pugal, K.J. Kim, and A. Aabloo, *Modeling the transduction of IPMC in 3D configurations*, in *Behavior and Mechanics of Multifunctional Materials and Composites 2010*, Vol. 7644 of *Proc. SPIE*, San Diego, CA, 2010, p. 76441T.

[28] D. Pugal, K.Jung, A. Aabloo, and K.J. Kim, *Ionic polymer–metal composite mechanoelectrical transduction: Review and perspectives*, Polymer Internat. 59 (2010), pp. 279–289.

[29] U. Zangrilli and L.M. Weiland, *Prediction of the ionic polymer transducer sensing of shear loading*, Smart Mater. Struct. 20 (2011), 094013:1–9.

[30] K. Takagi, M. Yamamura, Z. Luo, M. Onish, S. Hirano, K. Asaka, and Y. Hayakawa, *Development of a Rajiform swimming robot using ionic polymer artificial muscles*, in *Proceedings of the 2006 IEEE/RSJ International Conference on Intelligent Robots and Systems*, Beijing, China, 2006, pp. 1861–1866.

[31] Z. Chen, S. Shatara, and X. Tan, *Modeling of biomimetic robotic fish propelled by an ionic polymer–metal composite caudal fin*, IEEE/ASME Trans. Mechatronics 15 (2010), pp. 448–459.

[32] M. Aureli, V. Kopman, and M. Porfiri, *Free-locomotion of underwater vehicles actuated by ionic polymer–metal composites*, IEEE/ASME Trans. Mechatronics 15 (2010), pp. 603–614.

[33] W. Yim, J. Lee, and K.J. Kim, *An artificial muscle actuator for biomimetic underwater propulsors*, Bioinspiration and Biomimetics 2 (2007), pp. S31–S41.

[34] P. Brunetto, L. Fortuna, S. Graziani, and S. Strazzeri, *A model of ionic polymer–metal composite actuators in underwater operations*, Smart Mater. Struct. 17 (2008), 025029:1–12.

[35] K.J. Kim, D. Pugal, and K.K. Leang, *A twistable ionic polymer–metal composite artificial muscle for marine applications*, Marine Technol. Soc. J. 45 (2011), pp. 83–98.

[36] X. Tan, *Autonomous robotic fish as mobile sensor platforms: Challenges and potential solutions*, Marine Technol. Soc. J. 45 (2011), pp. 31–40.

[37] T. Ganley, D.L. Hung, G. Zhu, and X. Tan, *Modeling and inverse compensation of temperature-dependent ionic polymer–metal composite sensor dynamics*, IEEE/ASME Trans. Mechatronics 16 (2011), pp. 80–89.

[38] M. Aureli, C. Prince, M. Porfiri, and S.D. Peterson, *Energy harvesting from base excitation of ionic polymer–metal composites in fluid environments*, Smart Mater. Struct. 19 (2010), p. 015003.

[39] S. Samarasinghe, *Neural Networks for Applied Sciences and Engineering: From Fundamentals to Complex Pattern Recognition*, Auerbach, Boca Raton, FL, 2007.

[40] S. Coombs, M. Hastings, and J. Finneran, *Modeling and measuring lateral line excitation patterns to changing dipole source locations*, J. Comp. Physiol. A 178 (1996), pp. 359–371.
[41] N. Nguyen, D.L. Jones, Y. Yang, and C. Liu, *Flow vision for autonomous underwater vehicles via an artificial lateral line*, EURASIP J. Adv. Signal Process. (2011), 806406:1–11.
[42] NeuroSolutions http://www.neurosolutions.com/.
[43] K.J. Kim and M. Shahinpoor, *Ionic polymer–metal composites: II. Manufacturing techniques*, Smart Mater. Struct. 12 (2003), pp. 65–79.
[44] J.W.L. Zhou, H.Y. Chan, A.K.H. To, K.W.C. Lai, and W.J. Li, *Polymer MEMS actuators for underwater micromanipulation*, IEEE/ASME Trans. Mechatronics 9 (2004), pp. 334–342.
[45] G.H. Feng and R.H. Chen, *Fabrication and characterization of arbitrary shaped μ IPMC transducers for accurately controlled biomedical applications*, Sensors and Actuators: A Physical 143 (2008), pp. 34–40.
[46] E. Jacobsen and R. Lyons, *The sliding DFT*, IEEE Signal Process. Mag. 20 (2003), pp. 74–80.
[47] S. Shatara and X. Tan, *An efficient, time-of-flight-based underwater acoustic ranging system for small robotic fish*, IEEE J. Oceanic Eng. 35 (2010), pp. 837–846.